J. Mater. Eng. (1988) 10:143–162

Physical Metallurgy of Nickel-Base Alloys as It Relates to Corrosion

R.M. Latanision

Abstract. In service environments ranging from high purity water to deep sour gas, the corrosion and embrittlement characteristics of nickel-base alloys have been found to be intimately related to the physical metallurgy of the alloys. Intergranular corrosion, stress corrosion cracking, corrosion fatigue, and hydrogen embrittlement have been associated with, for example, grain boundary microstructure and microchemistry, solute segregation, ordering phenomena, and so on. This presentation will treat each of the abovementioned issues, and, in addition, consider improvements in corrosion resistance that may be expected through advanced processing, such as rapid solidification technology (RST).

1. INTRODUCTION

Physical metallurgy is that part of metallurgy that deals primarily with the evolution of microstructure, the corresponding structure–property relationships, the application and performance of metals and alloys under service conditions. It is, however, also much concerned with the relationship between processing and structure since all forms of processing strongly affect structure.

In service environments ranging from high purity water to deep corrosive sour gas, the corrosion and embrittlement characteristics of nickel-base alloys have been found to be intimately related, if however incompetely understood in many instances, to the physical metallurgy of the alloys. In this paper, a generic discussion of such structure–property relations will be presented by means of examples drawn by and large from work performed over a period of several years at MIT on topics such as intergranular corrosion, stress corrosion cracking, corrosion fatigue, and hydrogen embrittlement. While there is, of course, corresponding work performed elsewhere, the objective in this case is not to present an exhaustive review but, rather, to illustrate in a generic sense the role of physical metallurgy in the corrosion behavior of nickel-base alloys. Finally, consideration will also be given to the opportunity presented by advanced processing technologies, in particular rapid solidification processing, on improving the corrosion resistance of nickel-base alloys through control of alloy composition and microstructure in ways that are not tractable by more conventional (equilibrium) processing technologies.

The author is with the Department of Materials Science and Engineering, Massachusetts Institute of Technology, Cambridge, MA 02139.

2. THE INFLUENCE OF THERMAL TREATMENT ON CHEMISTRY AND STRUCTURE OF GRAIN BOUNDARIES IN NICKEL-BASE ALLOYS: INTERGRANULAR CORROSION

2.1 Aging Treatments at Elevated Temperatures

In this discussion, attention will be focused largely on Inconel 600, although similar phenomenology applies to other nickel-base and iron-base alloys as well. Alloy 600, a nickel-base alloy containing approximately 75 wt% nickel and 15 wt% chromium, is used extensively for pressurized water reactor (PWR) steam generator tubing. Because of its critical application in a high temperature aqueous environment, a great deal of interest has been focused on the effects that variations in thermal processing have on this alloy and its ability to resist environmental degradation at high temperatures. Particular emphasis has been placed on the chemistry that exists at or near grain boundaries. Carbide precipitation during thermal treatment can result in local chromium depletion and an accompanying degradation in corrosion resistance. A detailed microstructural study of age hardenable Inconel X-750

has been performed at MIT in relation to fatigue crack growth in boiling water reactor (BWR) environments and was presented at the ASM Conference on Corrosion of Nickel Base Alloys by Ballinger [1].

Three important processes occur during aging of Inconel 600 at temperatures between 500 and 800° C: Chromium carbides in the form of $M_{23}C_6$ or M_7C_3 precipitate at grain boundaries and this is accompanied by chromium depletion in the surrounding matrix. Similar sensitizing thermal treatments lead to intergranular corrosion in austenitic stainless steels. In addition, trace elements such as P, S, B, and Ti may segregate to the grain boundaries. These processes have been studied extensively by Was et al. [2] and the following is a summary of these findings. The paper by Thompson [3] considers as well the physical metallurgy of dispersion hardening and precipitation strengthening alloys not treated in the present paper.

Chromium carbides precipitate initially at grain boundaries. The diffusivity of carbon, which travels as an interstitial, is much higher than that of chromium which must diffuse substitutionally. This difference in diffusivities permits the formation of chromium carbides which then produces a chromium-depleted region surrounding the grain boundary. The extent of depletion is dependent upon such variables as temperature, time, and carbon content. The effects of these variables on the precipitation reaction can be illustrated in a time-temperature-transformation (TTT) diagram as shown in the schematic in Figure 1.

At any temperature, as time progresses, chromium replenishment (desensitization) of the grain boundary eliminates the depleted zone, and grain boundary carbides undergo restructuring to form more discrete particles. After long aging times, the chromium-depleted zone has been replenished, and any further carbide

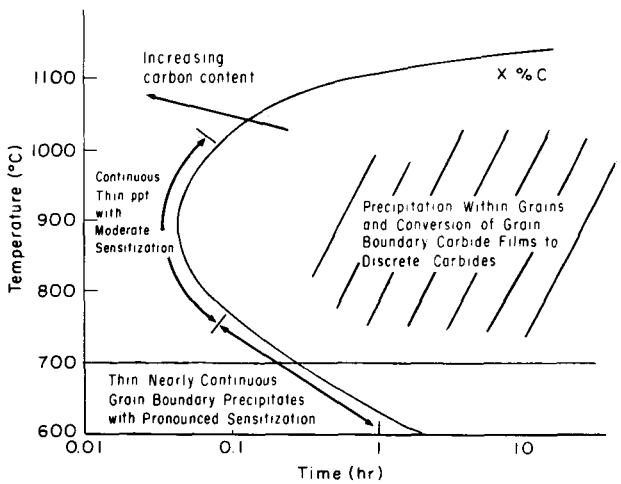

Fig. 1. Schematic of carbide precipitation diagram for Inconel 600 [2].

precipitation will occur within the grains. Hence the presence of grain boundary carbides is a necessary, but not a sufficient, condition for the occurrence of chromium depletion.

Considerable data exist in the literature documenting the segregation of impurities to surfaces and grain boundaries of Inconel 600 during thermal treating. However, the role of these impurities is the subject of considerable debate. Their presence has been linked to hydrogen embrittlement as well as to increased intergranular corrosion susceptibility. The first suggestion that such impurities act as hydrogen recombination poisons, thus stimulating hydrogen absorption at segregated grain boundaries, was made by Latanision and Opperhauser [4]. Armijo [5], Vermilyea et al. [6], and Brown [7] have shown that phosphorus and silicon can enhance intergranular corrosion in Inconel 600 and austenitic stainless steels. Guttmann claims that intergranular corrosion, which could not be due to the presence of a chromium-depleted zone (e.g., in nonsensitized stainless steels), is due to grain boundary segregation of trace elements [8].

The thermomechanical processing schedule for Inconel 600 steam generator tubing varies considerably among the various suppliers and, in addition, with time of initial service. Prior to 1978, most steam generator tubing was placed into service in a "mill annealed" condition. This tubing was representative of standard fabrication practice, and little or no attempt was made to optimize the microstructure with respect to in-plant performance.

Starting approximately in 1978 attempts have been made to optimize performance by microstructural modification. Microstructural optimization was achieved through thermal treatment after the final anneal to homogenize the grain boundary chromium concentration that was initially perturbed by carbide precipitation. A thermal treatment consisting of an age of approximately 15 h at approximately 700° C is representative of one such approach.

The results of the study of Was et al. [2] represent the first direct evidence of chromium depletion in Inconel 600 as a function of thermal treatment and are shown in Figures 2, 3, and 4. This work examined what may be called a solution anneal and sensitization (SAS) thermal treatment. All specimens were solution annealed at 1100° C for 30 min, water quenched, and then aged at various temperatures. Figure 2 is a scanning transmission electron micrograph of a specimen aged 100 h at 700° C. A temperature of 700° C was selected as the thermal treatment temperature for several reasons. First, 700° C falls on the approach to the nose of the TTT curve allowing better control of the time marking the onset of precipitation. Second, at this temperature the entire chronological process out-

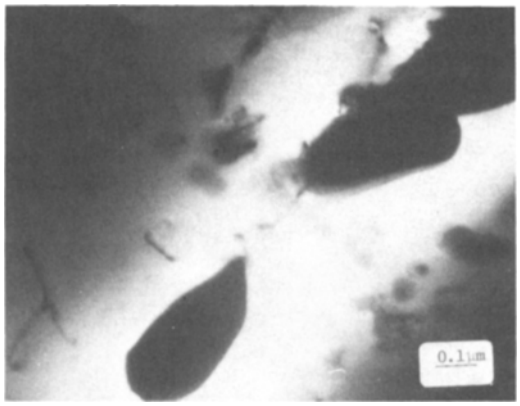

Fig. 2. STEM micrograph showing electron beam trace across a grain boundary and between carbides in a sample of Inconel 600 solution annealed at 1000° C for 0.5 h, water quenched, and subsequently aged at 700° C for 100 h [2].

lined above is complete in a reasonable amount of time (<100 h). Third, 700° C is a temperature at which grain boundary segregation of important trace elements, phosphorus and sulfur, has been shown to occur. Finally, at least one U.S. steam generator vendor thermally treats tubing at 700° C for approximately 15 h before placement in service, as described earlier.

The carbides in Figure 2 are spaced some 2000 A apart. The small dark circular spots are produced by contamination as the electron beam is stepped across the grain boundary between carbide particles, thereby allowing energy dispersive x-ray analysis of the grain boundary chemistry. Figure 3 shows a typical plot of the concentrations of chromium, iron, and nickel across

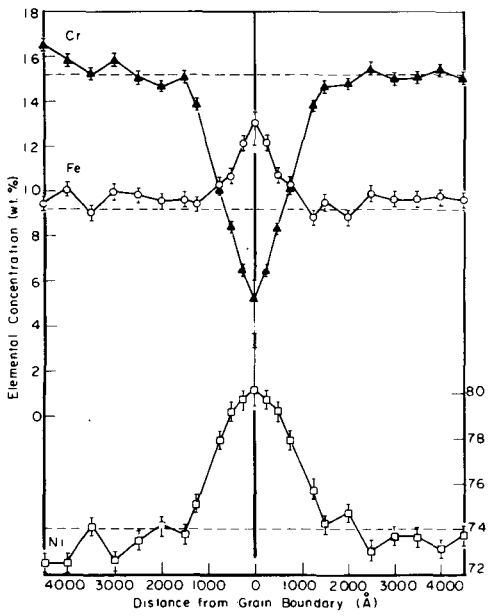

Fig. 3. Grain boundary chemistry of Inconel 600 aged for 5 h at 700° C following a solution anneal and water quench [2].

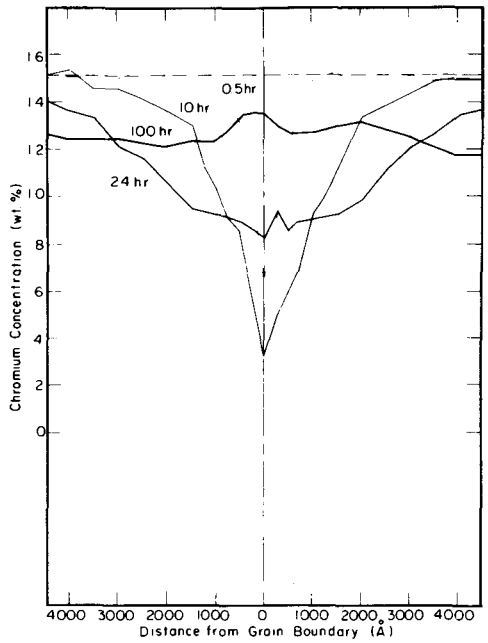

Fig. 4. Grain boundary chromium depletion in Inconel 600 aged for various times at 700° C following solution anneal and water quench [2].

a grain boundary in a sample thermally treated for 5 h at 700° C following a 30 min anneal at 1100° C. The horizontal dashed lines refer to the bulk concentrations of the respective elements as determined by chemical analysis. The concentrations calculated from STEM (Scanning Transmission Electron Microscope) analysis agree well with the chemical analysis at distances away from the depleted zone. One should also note that a decrease in chromium concentration is compensated by an increase in both iron and nickel concentrations with the larger contribution coming from nickel. It has been suggested that the decreased susceptibility to intergranular stress corrosion cracking in caustics may be associated with the increased grain boundary Ni content.

The chronological development of the chromium depleted zone is shown in Figure 4 for thermal treatments ranging from 0.5 to 100 h. Note that as the aging time increases, so does the width (and hence, volume) of the depleted zone. The maximum depletion is reached after 10 h at 700° C after which the depletion diminishes and the zone widens. After 100 h, the width of the depleted zone extends to approximately $^1/_{30}$ of a grain diameter. This is the longest thermal treatment analyzed and by this time the precipitation (and, hence, depletion) process is complete and only redistribution will occur with further aging until the bulk chromium level becomes uniform (and below the original level) throughout each grain, that is, a condition which may be described as that of a

desensitized microstructure. After this amount of time, precipitates have formed on the grain boundaries, twin boundaries, and dislocation pile-ups. From Figure 4, the minimum chromium content occurs after approximately 10 h at 700° C and results in a chromium concentration at the grain boundary of 3.3 wt%.

With respect to solute segregation in thermally treated Inconel 600, Was et al. [2] found that phosphorus exhibited the most consistent and reproducible behavior, appearing only on intergranular surfaces of samples thermally treated for 0.5 h or more. Figure 5 is a collage showing the distribution of phosphorus between intergranular and transgranular surfaces using an Auger line scan, an area map, and spot analyses. Note the precipitous drop in concentration where the line scan crosses the interface between inter- and transgranular surfaces. The intensity and density of white dots on the Auger map indicates that phosphorus is present only on the intergranular facets. Observe also from the spot analyses, the characteristic occurrence of high P and low S contents on intergranular facets (top scan) and high S and no P on transgranular facets (bottom scan) after 10 h at 700° C. In short, except for P, the grain boundaries in Inconel 600 are not exclusive sinks for trace element segregation at 700° C.

Figure 6 illustrates the dependence of the intergranular corrosion susceptibility of Inconel 600 on thermal treatment as determined by the Huey (boiling HNO_3) and Streicher tests (boiling H_2SO_4 and $Fe_2(SO_4)_3$). The highest corrosion rate occurs after aging for 10 h at 700° C which corresponds, as mentioned above, to the maximum chromium depletion, al-

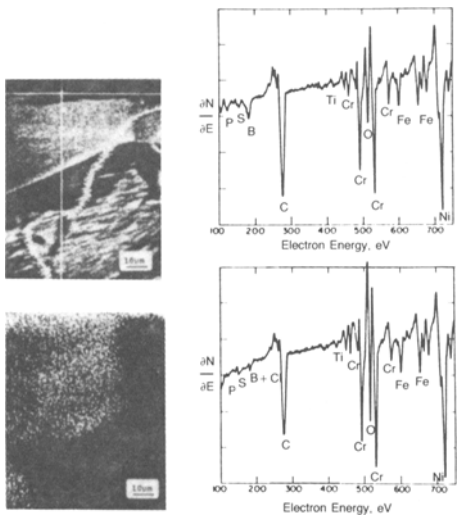

Fig. 5. Phosphorus concentration on inter- and transgranular fracture facets using an Auger line scan (top left), area map (bottom left), and spot analyses (right). The phosphorus concentration increases from left to right in the line scan [2].

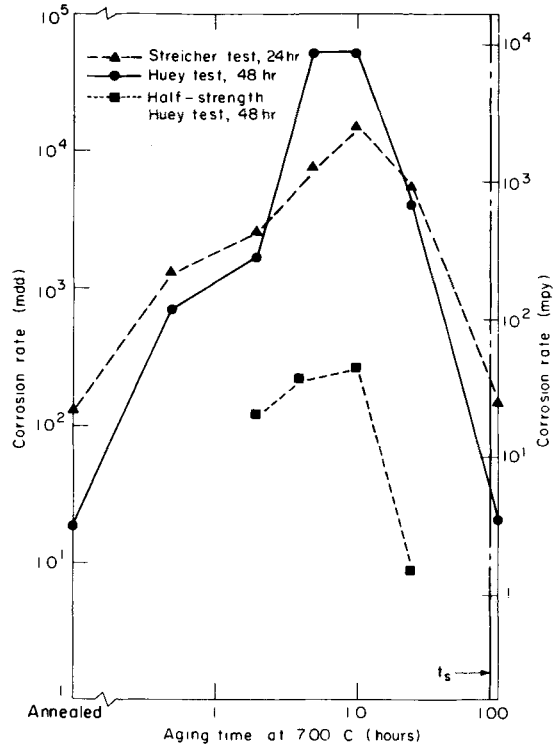

Fig. 6. Intergranular corrosion of Inconel 600 as a function of thermal treatment as measured by the Huey and Streicher tests [2].

though the results of this work suggest that preferential corrosion at grain boundaries occurs when the chromium level falls below 9%. This value is also the self-healing level of chromium in Inconel 600. Since the intergranular corrosion rate varied radically as a function of thermal treatment, whereas the grain boundary concentration of these elements did not, it is most likely that the intergranular corrosion behavior is a result of chromium depletion rather than impurity segregation. But since this segregation was rarely present without chromium depletion, Guttmann's claim [8] that intergranular corrosion in nonsensitized Inconel 600 is due to segregation of phosphorus and silicon to grain boundaries can neither be substantiated nor refuted by these results. Others, [9–11] including Jones et al. [9], have examined the intergranular corrosion of nickel [9] and iron-based stainless steels [10,11]. In the latter, it is found that segregated phosphorus does lead to intergranular corrosion of nonsensitized [10] and sensitized [11] austenitic stainless steel in highly oxidizing media.

2.2 Low Temperature Aging

As described above, the kinetics of the grain boundary chromium depletion process has been studied for both iron- and nickel-base alloys and has been found to be driven by the formation of chromium carbides.

As carbides nucleate and grow, they act as sinks for the surrounding chromium. This results in a zone adjacent to the grain boundaries that is depleted in chromium. The initial reaction occurs quickly at 700° C and leaves this region chromium poor. As the carbides grow, however, their rate of growth decreases with the decline in the activity of carbon. Eventually, chromium will diffuse back into the depleted region and homogenize or desensitize the material. For aging at 700° C, depletion and subsequent homogenization of chromium may take a day to occur, while at lower temperatures the process can take substantially longer.

The operating temperature that Inconel 600 tubing experiences in service in light water reactors is approximately 315° C. Although this temperature is quite low with respect to the kinetics of the chromium depletion process, the long service life, approximately 50 years, has raised questions as to whether material which is susceptible to chromium depletion will experience this effect while in service. There is conflicting evidence regarding the answer to this question in the literature. Low temperature aging studies on Inconel 600 have, for some studies, shown little evidence of chromium depletion for aging times up to 15,000 h. Airey [12] aged several different heats of mill-annealed material and found that for tubing aged below 480° C, no substantial depletion in grain boundary chromium could be found as indicated by a boiling nitric acid test. This result is in contrast with the work by Ljungberg [13]. Ljungberg's work on 304 stainless steel suggests that, given a proper prior treatment to induce carbide nucleation, subsequent low temperature aging will result in additional chromium depletion. He found that a thermal pretreatment of 800° C for 1 h was sufficient to induce carbide nucleation in his material. His results implied that in order for significant depletion of chromium to occur at low temperatures, the material must have been given a prior treatment to "seed" the grain boundaries with small carbide nuclei. Under these circumstances subsequent further precipitation and growth with accompanying chromium depletion is likely during lower temperature aging.

As a result of the aforementioned concerns, we have undertaken a study [14] to evaluate the susceptibility of Inconel 600 to grain boundary sensitization when aged at temperatures ranging from 300 to 600° C. Specimens of Inconel 600 in the mill annealed and thermally treated (aged additionally at 700° C for 15 h after the mill anneal) were examined. The carbide morphology of both specimens appeared similar: a semi-continuous grain boundary network with additional intragranular carbide precipitates. However, the response of the two initial conditions, mill annealed and thermally treated, to subsequent thermal aging was quite different. The thermally treated material did not respond at all to a modified Huey test while the mill annealed material did. The thermally treated material exhibited a weighted loss of 0.004 mg/cm^2/day independent of thermal aging, while for the mill annealed materials weight loss was a function of aging time and temperature. Figure 7 shows the results of the aging study for the mill annealed material in the form of a TTT diagram. Corrosion values in mg/cm^2/day are listed below each symbol. The degree of intergranular attack (IGA) was determined by sectioning each sample after the test and evaluating the degree of penetration with a light microscope at 100 ×. Partial IGA was defined as a penetration depth of approximately one grain.

The mill annealed material exhibited a baseline weight loss of approximately 0.4–0.6 mg/cm^2/day. In addition, the peak in weight loss occurred for an aging treatment of 500° C for 100 h. For aging treatments above this temperature no additional weight loss beyond the baseline was observed. For aging below 500° C the trend was for weight loss to increase with time with an absence of the peaked behavior observed for the 500° C aging. Figure 8 shows micrographs of the mill annealed material after the following treatments: (a) aging at 300° C for 10,000 h; (b) unaged; (c) solution treated at 1150° C for 15 min. When compared to the unaged and solution treated materials, there is clear evidence of intergranular corrosion when mill annealed Inconel 600 is aged at 300° C for 10,000 h. In general, an increased degree of IGA as indicated by corrosion tests corresponded to a decrease in grain boundary chromium concentration as observed by STEM (Table 1).

For all but one case the level of grain boundary chromium concentrations was found to be significantly below the bulk chromium concentration. The

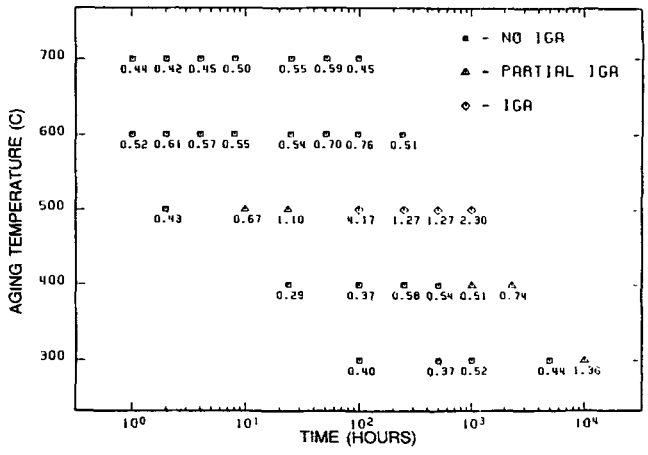

Fig. 7. TTT diagram for mill annealed Inconel 600 which has been aged. Partial IGA is attack which is one grain or less deep [14].

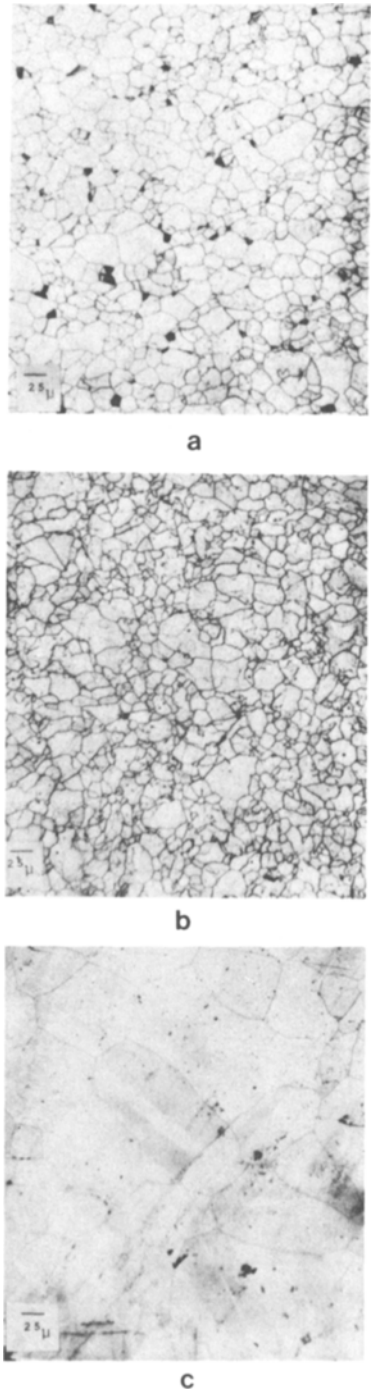

Fig. 8. Micrographs of mill annealed Inconel 600 after (a) aging at 300° C for 10,000 h; (b) unaged; and (c) solution treated at 1150° C for 15 min [14].

parameter f/σ_f in Table 1 is the ratio of the difference between mean grain boundary and matrix chromium concentrations, f, and the standard deviation of f, σ_f. The parameter is a measure of the overlap between the boundary and matrix distributions, assuming normal behavior. For the sample that exhibited the most severe IGA in the nitric acid test, the degree of chromium depletion was also found to be greatest. Unaged mill annealed material was also found to have a slightly depressed level of grain boundary chromium, but significantly above the aged material. The sample aged at 300° C for 10,000 h showed grain boundary chromium concentrations well below that of the matrix and significantly below that of the unaged material. Data for this sample were taken from over 100 grain boundaries. The implication, therefore, is that for chromium levels below 12% the material will become susceptible to IGA in a standard test, the Huey test.

There is, however, evidence, as mentioned earlier, that segregated phosphorus will cause an increase in the IGA of Inconel 600. Auger electron spectroscopy (AES) was used to study grain boundary phosphorus levels of Inconel 600 specimens fractured in the Auger spectrometer chamber. Evidence of grain boundary phosphorus did exist, at levels of up to 2.5%. However, the concentration of phosphorus at grain boundaries remained at the levels typical of mill annealed material in the unaged condition regardless of the aging temperature. This was to be expected, since the diffusion of phosphorus below 500° C is very slow. Using the data by Guttman [8] and extrapolating to 300° C, the diffusion coefficient of phosphorus is on the order of 10^{-24} m^2/s. Significant diffusion of phosphorus to the grain boundaries would be a very slow process, and unlikely in 10,000 h. In this case, increased attack in the nitric acid test for the mill annealed material that had been aged for 10,000 h at 300° C cannot be due to a change in the phosphorus concentration, but is more likely due to a drop in the grain boundary chromium level.

The aforementioned behavior may be understood using the model of Stawstrom and Hilbert [15] which describes the thermodynamics of carbide growth. In their work, it is assumed that the growth of the carbide is controlled by the local equilibrium at the carbide/austenite interface. In this case the concentration of chromium and carbon at the interface are determined by the activity of carbon. The conditions at the interface are thus uniquely defined by the carbon activity. As the carbides begin to precipitate at the grain boundaries, the local carbon activity diminishes. The initial concentration of chromium drops significantly due to formation of the carbides, prompting chromium to diffuse to the growing carbide. According to Hilbert, the material is assumed to become sensitive to an oxidizing environment once the width of the depleted zone reaches a critical value of 200 Å.

If the processes are stopped and allowed to continue at a lower temperature, as would be the case for the in-service situation, the activity of carbon will be

Table 1. STEM analysis of Inconel 600 tubing as a function of aging treatment [14]

Aging Treatment	Nitric Acid Test	STEM Analysis[a] GB	STEM Analysis[a] Matrix	f/σ_f
As received	Etch	13. ± 0.8	14.1 ± 0.4	1.11
500° C 100 h	Heavy attack	11.5 ± 0.8	14.1 ± 0.4	2.89
400° C 2250 h	Light attack	12.7 ± 1.1	13.8 ± 0.8	0.786
300° C 5000 h	Etch	13.2 ± 1.3	14.1 ± 0.3	0.692
300° C 10000 h	Light attack	12.7 ± 0.6	14.1 ± 0.2	2.33

[a]Percentages listed are in weight percent.

initially higher and the interface chromium will tend to fall accordingly. Precipitation and depletion continues, except now at the lower temperature the characteristics of the chromium-depleted zone are controlled by the diffusion of chromium. The process thus takes much longer. Assuming a diffusion coefficient of 10^{-24} cm^2/s for chromium in Inconel 600 at 300° C, the time needed to reach sufficient depletion for a response from the nitric acid test would take many years. This does not mean, however, that depletion is not occurring on a scale that would be detected by more sensitive means such as STEM.

Raising the aging temperature would result in a decrease in the carbon activity. No new depletion would occur and healing would continue and take less time since the diffusion coefficient of chromium would be higher at the higher temperature.

This scenario of events is in agreement with the model proposed by Stawstrom and Hilbert for chromium depletion. Whether a material will continue to undergo depletion and precipitation depends on the initial state of the grain boundaries; hence the previous processing history, prior to aging. The effect of low temperature aging will thus only be observed for material whose boundaries have been preconditioned by a prior age at higher temperature of sufficient length to cause carbide nucleation and growth but minimal healing. For these conditions, chromium depletion can occur at low temperature in relatively short periods of time. The results of this study are in agreement with the conclusion of Ljundberg [13] in that the effect of low temperature aging can only be in evidence when the material is given a heat treatment that will induce the low temperature effect. The material used in this study was partially depleted at the outset, and subsequent aging produced the increased grain boundary dissolution in the nitric acid test.

3. ENVIRONMENTALLY-INDUCED EMBRITTLEMENT OF N-BASE ALLOYS

Physical metallurgy plays an intimate role in the environmentally induced embrittlement of nickel-base alloys, although, however, our understanding of this important structure-property relationship is far from complete. Current reviews of stress corrosion cracking [16,17], corrosion fatigue [18], and hydrogen embrittlement [19] of nickel-base alloys is given. As such, no attempt will be given here to examine each of these complex topics in detail, but short summaries follow.

3.1 Corrosion Fatigue

Fatigue crack growth of nickel-base alloys in aqueous systems is relatively less studied than other forms of embrittlement. There is, however, some incentive to pursue this issue from the point of view of nuclear systems. The conditions in a steam generator are such that a tube may be subjected to fatigue from fluid flow, thermal stresses, and pressure fluctuations. This leads to load cycles that may vary in frequency from $10^2 s^{-1}$ (flow vibrations) to $10^{-7} s^{-1}$ (shutdown-startup associated loads). With nearly sixty miles of tubing per steam generator, the presence of flaws prior to startup is inevitable. Combined with an aggressive environment and a susceptible microstructure, considerable enhancement of the fatigue crack growth rate may result.

Since the Inconel 600 tubes in present-day steam generators pass through carbon steel support plates, a galvanic cell may be established upon contact. Although the local environment in a steam generator may vary significantly, the possibility exists that at operating temperatures and pressures the Inconel 600 tube is cathodic relative to the carbon steel support plate. At room temperature, Inconel 600 is cathodic relative to carbon steel and the reduction of protons to form atomic hydrogen on the tube surface is the likely cathodic reaction, particularly in deaerated water. Adsorbed atomic hydrogen can either combine to form molecular hydrogen, or become absorbed into the metal. This uncombined or atomic hydrogen may be a possible source of embrittlement.

Was et al. [20] have examined the fatigue crack growth of Inconel 600 as a function of applied potential, test frequency, and prior thermal history in

aqueous H_2SO_4 under conditions of ambient temperature and pressure. At an applied cathodic potential of −700 mV (Saturated Calomel Electrode (SCE)), in 1 N H_2SO_4, a decrease in test frequency produces an increase in crack growth, da/dN, while a thermal treatment of 700° C for 0.5 h or more following solution annealing produces intergranular fracture at low ΔK. Intergranular cracking of annealed samples was observed only after precharging with cathodically produced hydrogen. The enhanced fatigue crack growth (FCG) rate and tendency for intergranular cracking are mutually exclusive effects in that test frequencies between 1 and 10 Hz do not affect the fracture mode, and thermal treatment at 700° C for 0.5 to 100 h does not affect crack growth rate. The latter is shown in Figure 9. A variety of thermal treatments were examined under the same conditions to assess their effect on FCG rate. Figure 9 shows that there is essentially no difference between the crack growth rate in annealed specimens and those thermally treated for 0.5, 10, and 100 h at 700° C (A0.5, A10, A100, respectively). These thermal treatments span the spectrum of grain boundary conditions from clean (annealed) to highly sensitized (10 h), to healed or desensitized (100 h). The fatigue crack growth rates show very little difference in magnitude in the range $33 < \Delta K < 55$ MPa $\sqrt{m}$.

The fracture surfaces of all thermally treated specimens tested at cathodic potentials was characterized by intergranular fracture at low ΔK, followed by transgranular fracture at higher ΔK. Figure 10 shows a FCG curve with a superimposed fracture surface sketch and fractographic display. This specimen was in the A10 condition and tested at 1 Hz, −700 mV (SCE) and R = 0.05. The bowed shape of the front delineating the regions between mixed mode fracture and purely transgranular fracture indicates that potential control was lost first at the center of the specimen. As the crack growth rate and ΔK increase, the fracture mode gradually changes to transgranular across the entire cross section. It should be noted that the transition from intergranular to transgranular is not sharply defined but occurs gradually over a distance of perhaps 1 mm. The transition lines have been drawn at an intermediate position.

In summary, the following observations have been documented:

1. Acceleration of the fatigue crack growth rate as the frequency decreases when specimens of annealed or aged conditions are charged at −700 mV (SCE) during testing.
2. Intergranular fracture in all thermally treated spec-

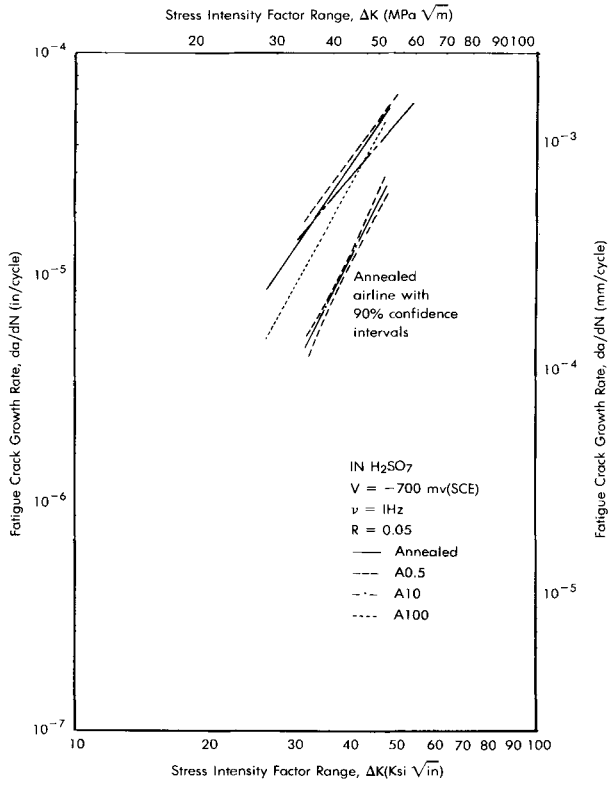

Fig. 9. Effect of thermal treatment on the fatigue crack growth behavior of Inconel 600 in 1 N H_2SO_4 at an applied potential of −700 mV(SCE) and a test frequency of 1 Hz [20].

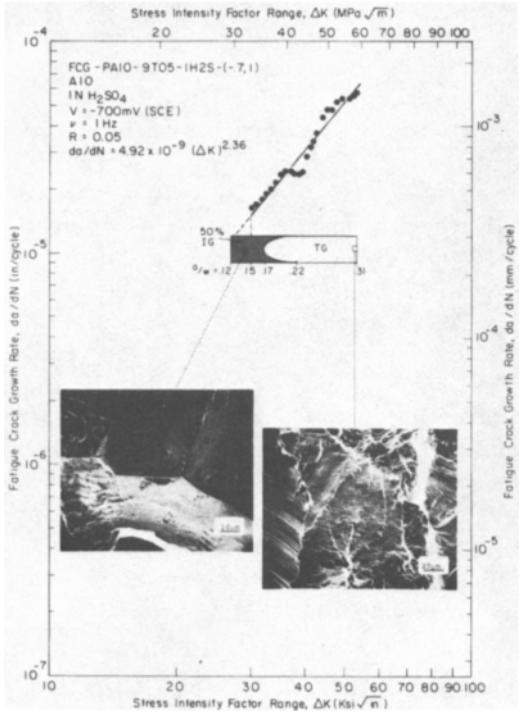

Fig. 10. Fatigue crack growth behavior of Inconel 600 in I N of H_2SO_4 at an applied potential of −700 mV(SCE) and a test frequency of 1 Hz [20].

imens, independent of test frequency, when charged at −700 mV (SCE) during testing. Only transgranular cracking was observed in solution annealed specimens which were unaged, except for those precharged with hydrogen.

3. Intergranular fracture at shallow depths below the specimen surface in solution annealed samples precharged with hydrogen and tested under open-circuit conditions.

It is unlikely that chromium depletion has any effect on the observed results. This claim is largely supported by a lack of observable differences in either the crack growth rate or fracture morphology even though the extent of chromium depletion varies significantly between thermal treatments. Intergranular embrittlement as well as an increase in fatigue crack growth rate was observed to be of similar magnitude in all thermally treated specimens. Intergranular fracture in thermally treated specimens could be a result of impurity segregation. Phosphorus is the only impurity that consistently segregates to the grain boundary in all thermal treatments but is absent after annealing. The tendency of hydrogen to cause intergranular embrittlement in the presence of phosphorus in nickel-base alloys will be described subsequently and is a likely possibility for the cause of intergranular crack growth observed here. Was et al. [20] postulated that hydrogen is responsible for both the enhanced fatigue crack growth rate and intergranular cracking. Although the presence of phosphorus and/or chromium carbides at the grain boundaries of thermally treated samples correlate with intergranular cracking, more than this casual relationship has not been verified. Hence, no definitive conclusion can be made concerning the mechanism of hydrogen embrittlement in Inconel 600.

Ballinger [21] and Moshier [22] have examined the fatigue behavior of Inconel 600 at 288° C in air-saturated and deaerated pure water as a function of metallurgical and mechanical parameters. The results of these tests may be summarized as follows:

1. Sensitization in Inconel 600 appears to have very little effect on the fatigue behavior of this material in aerated high purity water (0.2 ppb dissolved oxygen). However, increasing the amount of dissolved oxygen can increase the crack growth rate. This is shown in Figs. 11 and 12, in which the sensitized alloy was solution annealed and aged at 700° C for 2 h while the desensitized alloy was aged for 120 h.
2. Cathodic charges showed little effect on growth rate, regardless of the aging treatment, in high temperature water; this was in contrast to the findings of Was et al. [20], in 25° C sulfuric acid. There

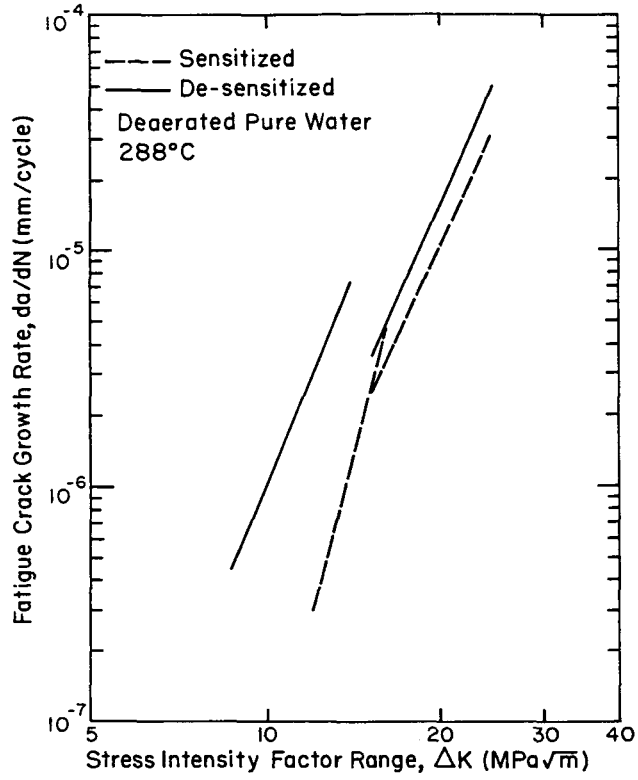

Fig. 11. Summary of fatigue crack growth tests conducted in deaerated (2 ppb/oxygen) pure water at 288° C [22].

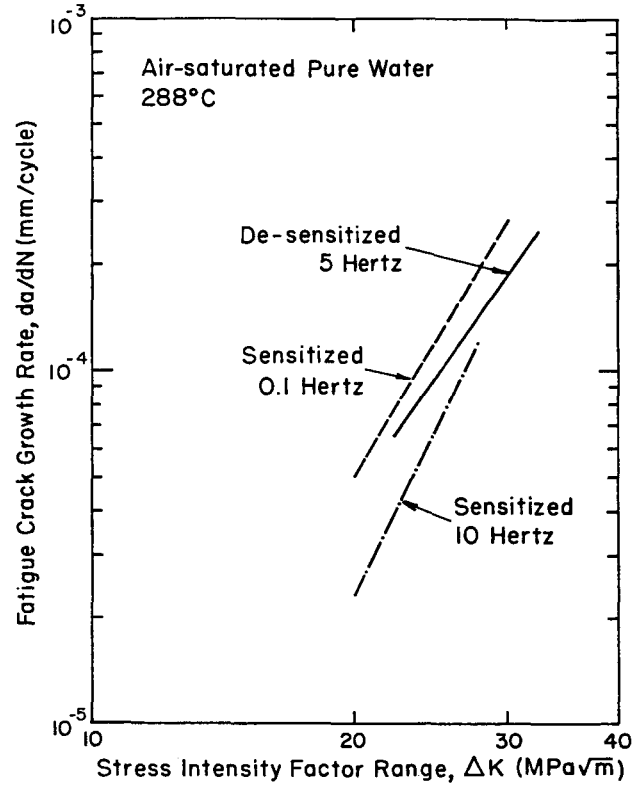

Fig. 12. Summary of fatigue crack growth tests conducted in air-saturated pure water at 288° C [22].

was no observable increase in the crack growth rate and no change in crack morphology.

3. The crack path was largely transgranular in both sensitized and desensitized alloys. The desensitized material, however, had a greater degree of intergranular fracture than the sensitized material. No intergranular fracture was observed in sensitized Inconel 600 at elevated temperatures and pressures.

Similar work on X750 in simulated BWR environments is described by Ballinger [1].

3.2 Stress Corrosion Cracking

Interest in the intergranular stress corrosion cracking of nickel-base alloys has been stimulated in recent years by the nuclear power generation industry [23–25] and by the oil and gas production industry [26]. In both cases stress corrosion cracking (SCC) is known to be affected by microstructural characteristics.

In the case of the nuclear industry, SCC has been reported in high temperature (300° C), high purity water [23–25] in caustics [23–25] and, more recently, in low-temperature sulfur-bearing environments [27]. While the volume of research on SCC of Inconel 600 is extensive, the mechanism of cracking is still unclear. A susceptible structure is now generally associated with carbide-free grain boundaries as first pointed out in the work of Blanchet et al. [28] (Table 2). Semicontinuous grain boundary precipitates appear effective in preventing intergranular SCC in caustic, pure water, and in sulfur-bearing environments [27]. This is, of course, something of a reversal of the intergranular SCC dependence of austenitic stainless steels on microstructure. Although the detailed dependence on thermal treatment is different for the case of SCC in high purity water environments (solution annealed specimens are very susceptible while sensitized grades are more resistant) and for the case of SCC in S-bearing environments (solution annealed specimens are essentially immune but sensitized material is most susceptible), both types of SCC are reduced by thermal stability of Inconel 600 [27]. Appropriate (thermal stabilization) treatments, for example, Airey's proposal [29] of thermal treatment at 982–1010° C for 1 to 5 min followed by 704° C for 15 h, apparently lead to maximum resistance to SCC. Treatment of the alloy to conditions well within the precipitation region of the TTT diagram (Fig. 1) results in semicontinuous grain boundary precipitates and replenishment (desensitization) to some extent of the chromium-depleted layer presumably affecting the cracking susceptibility. Such thermal stabilization (TS) treatment is expected to largely overcome the problem of wide heat-to-heat variability in mill annealed materials [30]. Although the mechanism of SCC in high-temperature water environment remains a matter of much debate, Bandy and Van Rooyen [25] recently concluded that SCC occurs in simulated PWR water at potentials cathodic to the corrosion potential, perhaps a consequence of absorbed hydrogen, and at anodic potentials, controlled by a film rupture mechanism.

The high strength and excellent resistance to corrosion of high performance (Ni–Cr–Mo) alloys such as Hastelloy C-276 [31–35] and Inconel X750 [36] are attractive characteristics of materials of construction in deep sour oil and gas wells. Although these alloys were originally intended for service in high-temperature applications (aircraft, aerospace, etc.), they are becoming widely used in hostile aqueous environments. Deep sour gas wells contain, in addition to hydrocarbons, acid gases such as CO_2, H_2S, and various brine components at temperatures up to 450° F and at pressures often in excess of 20 ksi (138 MPa). It was once considered that such high nickel-base alloys were resistant to chloride-induced transgranular stress corrosion cracking. Recent work, however,

Table 2. Fraction of Inconel 600 specimens cracked as a function of exposure time in high purity water. No cracking was observed under operating conditions for the sensitized material (1 h at 700° C followed by quenching) [28].

	Alloy A Inconel 600, C = 0.063			Alloy B Inconel 600, C = 0.040			Alloy C Cr 17%, Ni77% C = 0.002	
Samples cracked after	As Received	As Quenched	Sensitized	As Received	As Quenched	Sensitized	As Received	Sensitized
750 h	0/6	0/3	0/3	0/3	0/2	0/2	6/7	0/5
1500 h	6/6	0/3	0/3	0/3	0/2	0/2	7/7	3/5
2250 h		0/3	0/3	1/3	0/2	0/2		5/5
3000 h		0/3	0/3	2/3	0/2	0/2		
4500 h		1/3	0/3	2/3	0/2	0/2		
8250 h		1/3	0/3	3/3	0/2	0/2		
10000 h		2/3	0/3		1/2	0/2		

shows that these alloys are susceptible to such embrittlement in high temperature (400° F, National Association of Corrosion Engineers (NACE) solution–5% NaCl, 0.5 acetic acid, saturated with H_2S) chloride environments [31,33,34]. In addition, such alloys appear to be susceptible to low-temperature intergranular hydrogen embrittlement in 25° C NACE solutions [31–36]. Moreover, resistance to hydrogen embrittlement and to (chloride) stress corrosion cracking appears to have quite different functional dependences on metallurgical history. In short, resistance to hydrogen-induced cracking does not necessarily correlate with resistance to (chloride) stress corrosion cracking. In fact, it appears that in the case of deep sour gas wells, for example, there is no single material which resists both hydrogen embrittlement and SCC at the strength levels desired.

The hydrogen embrittlement of Hastelloy C-276 has been of particular interest recently [31–36]. Berkowitz and Kane [31], for example, have shown that embrittlement susceptibility is increased by aging treatment conducted within the range of 200–500° C (Table 3). No failures were observed in specimens which were not galvanically coupled to mild steel, implicating hydrogen as a prerequisite to failure. Interestingly, similar observations were reported by Blanchet et al. [28] with respect to the intergranular cracking of Inconel 600 in high-temperature water; contact with noble metals reduced susceptibility whereas contact with carbon steel accelerated cracking. Moreover, embrittlement resistance decreased with the time or temperature of the aging treatment: Short times at high temperatures or longer times at low temperatures decrease resistance to embrittlement. Cold worked specimens which were unaged were found to exhibit adequate resistance to intergranular embrittlement.

There is concern, therefore, that cold worked alloys (sufficient strength) may age and embrittle in service at downhole temperatures. Based on the increasing evidence of the effect of tramp impurities on environmentally induced embrittlement [4], it was hypothesized that grain boundary impurity segregation may be playing a role. Thus, samples of Hastelloy C-276 were charged cathodically with hydrogen and then fractured in vacuum. Scanning Auger spectroscopy was used to determine the grain boundary composition of the unaged and aged specimens. The Auger results revealed considerable phosphorus segregation to the grain boundaries which correlated with the aging treatments. Experimental low phosphorus heats were tested in the same environment and showed improved resistance to embrittlement when bulk phosphorus levels were lowered significantly below com-

Table 3. The effect of aging on the embrittlement susceptibility of Hastelloy C-276 tubulars in NACE solutions (25° C, C-ringes/steel coupled) [31].

Condition	Aging Temperature (C)	Aging Temperature (F)	Aging Time (Hours)	Time to Failure (days) 100% Trans. YS	Time to Failure (days) 90% Trans. YS
	Unaged		—	100[a]	100[a]
37% Cold reduced tubular	149	300	339	100[a]	—
	204	400	339	11	—
			535	—	100[a]
	371	700	20	<3	—
	482	900	0.16	<3	—
	482	900	100	<3	
	Unaged		—	100[a]	100[a]
48% Cold reduced tubular	149	300	339	4	—
			607	—	100[a]
	204	400	339	6	—
			535	—	100[a]
	371	700	20	<3	—
	482	900	0.16	<3	—
	482	900	100	<3	
	Unaged		—	100[a]	—
59% Cold reduced tubular	149	300	258	100[a]	—
			266	—	100[a]
	204	400	252	4	
			266	—	29
	371	700	20	<3	—
	482	900	0.16	<3	—
	482	900	100	<3	

[a]Specimens were removed from test after specified time, no failure.

mercial levels. The results of this investigation suggest a relation between the hydrogen embrittlement of this alloy and phosphorus segregation at the grain boundaries. The possible role of such impurities will be discussed in the next section.

It should, of course, be mentioned that while the hydrogen embrittlement susceptibility of such Ni–Cr–Mo alloys has been often studied [31–36], the mechanism by which cracking occurs remains the subject of considerable controversy. As indicated above, one school [31] showed that aging caused segregation of P to the grain boundaries and that embrittlement is associated with the electrocatalytic action of P in stimulating hydrogen absorption. Another school [32–35], on the other hand, has suggested that ordering, which occurs upon aging, prompts planar slip and may in turn enhance crack nucleation at emergent slip steps, increase internal stress concentration at dislocation pile-ups and/or promote transport of hydrogen by a dislocation drag mechanism.

3.3 Hydrogen Embrittlement

3.3.1 Segregated Impurity—Hydrogen Interactions. The importance of impurity segregation at internal interfaces, particularly grain boundaries, in the phenomenology of various forms of embrittlement—temper embrittlement [37], stress corrosion cracking [38], and so on—had been proposed some time ago. More recently, surface analytical tools, such as Auger electron spectroscopy, have made it possible to substantiate such proposals. For example, temper embrittlement of steels appears related to the grain boundary accumulation of alloying elements such as Ni and Cr and impurity elements (metalloids) such as P, Sb, and Sn [39–42]. Intergranular embrittlement of W [43], Cu [44], and phosphor bronze [45] have been associated with segregated P, Bi, and P, respectively. In many cases embrittlement has been attributed to a reduction in (grain boundary) surface energy, a consequence of the segregation of solutes to the grain boundary. There are instances [46], however, where grain boundary solute segregation is found to induce ductility in polycrystalline specimens that would fail intergranularly in the absence of such segregation. The latter is, of course, not attributable to a Gibbsian reduction of grain boundary energy. Similarly, galvanic effects in electrolytes arising out of chemical inhomogeneity between grain boundaries and contiguous grains have also been considered a source of intergranular failure [38]. Depending on the nature of the impurity element, increased or decreased reactivity may be expected to occur as a consequence of segregation. In the following, attention will be focused on the part played by segregated impurities in the intergranular hydrogen embrittlement of nickel and nickel-base alloys.

Impurities may play an important role in embrittlement induced by cathodically produced hydrogen, particularly if the segregated species happen to be metalloids such as those mentioned previously which are known to be effective catalytic poisons for the hydrogen recombination reaction in electrolytes. The significance of recombination poisons was first pointed out by Latanision and Opperhauser [4] in a study of the intergranular embrittlement of nickel by cathodically produced hydrogen. Perhaps the most effective way to examine the influence expected of metalloid elements on cathodic kinetics is to consider Fig. 13, which shows the exchange current density for hydrogen evolution for some of the elements in the periodic chart. The exchange density may be considered a measure of the catalytic efficiency of a given element for the hydrogen evolution reaction at the reversible potential. Notice that the exhange current density for the hydrogen reaction is orders of magnitude higher on noble metals (typically 10^{-3} A/cm^6) or other transition metal surfaces (10^{-6} a/cm^2) than on metalloid surfaces (10^{-13} A/cm^2). The overall hydrogen evolution reaction may be broken down into, for example, a proton reduction step, $H^+ + e = H_{ads}$, and a hydrogen adatom–adatom combination step. Metalloid elements effectively poison the reaction, $H_{ads} + H_{ads} = H_2$, thereby increasing the population of adsorbed, uncombined hydrogen on the electrode surface and, consequently, the probability that atomic hydrogen will be absorbed by the metal also increases. The influence of soluble metalloid salts in increasing the absorption of hydrogen from electrolytes at cathodic potentials is well documented [47–48]. Hence, as suggested by Latanision and Opperhauser [4], one might expect metalloid-segregated grain boundaries to act as preferential sites for the absorption of cathodic hydrogen into polycrystalline metals, Fig. 14. In essence, it may be argued that the entry

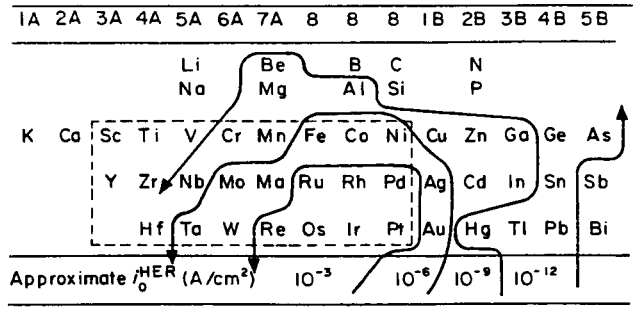

Fig. 13. The exchange current density for the hydrogen evolution reaction, i_o^{HER} for various elements in the periodic chart.

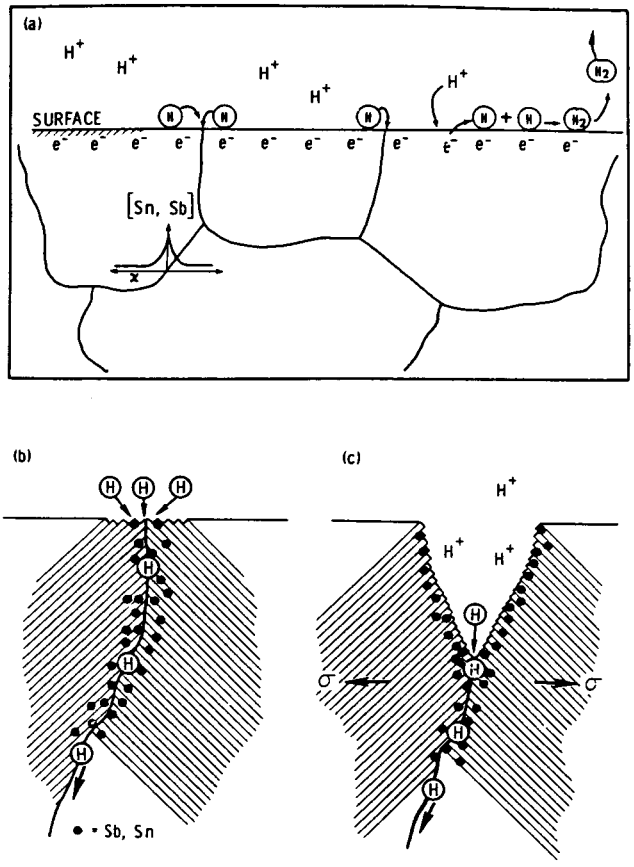

Fig. 14. Schematic indicating the preferential absorption of atomic hydrogen along metalloid-segregated grain boundaries and subsequent intergranular embrittlement of polycrystalline nickel [4].

of hydrogen into nickel occurs preferentially in the proximity of the grain boundary intersections with the free surface due to the presence therein of metalloids which act to poison the combination of hydrogen atoms formed by the discharge of protons from the electrolyte. At locations remote from the grain boundary, protons are reduced forming hydrogen adatoms which in the absence of a poison have a high probability of combining to form molecular hydrogen and are, thus, subsequently evolved. In the vicinity of a grain boundary, in contrast, rather than evolving from the electrode surface in molecular form, uncombined hydrogen atoms increase in number at the interface, and the probability of their absorption into the metal lattice increases.

It should be appreciated that the embrittlement of nickel described previously is not the result of segregation of metalloids alone, as indicated by the fact that identical tensile specimens deformed in the absence of hydrogen were not embrittled. Indeed embrittlement is associated with the interaction between segregated species and the surrounding environment. Such impurity–microchemistry interactions may apply to other metals and alloys as well. Grain boundary segregation of phosphorus, for example, has been observed in thermally treated nickel-base alloys such as Inconel 600 and Hastelloy C-276, both of which are subject to intergranular hydrogen embrittlement as described earlier. Likewise, recent extensive work by Bruemmer et al. [49] has shown a similar fracture mode transition in hydrogen-charged iron and nickel as a function of grain boundary sulfur segregation. It is in fact interesting that in the work by Bruemmer et al. [49] it is found that while the accumulation of segregated sulfur at grain boundaries in nickel reduces ductility in the presence of hydrogen, segregated phosphorus reduces the tendency for hydrogen-induced intergranular embrittlement. While both S and P should be expected to behave similarly from an electrocatalytic point of view (both should stimulate hydrogen absorption), it is important with respect to embrittlement to recognize that the electrocatalytic behavior of such elements must be separated from their role in the solid state chemistry of bonding interactions. In short, there is no a priori reason to expect elements that stimulate hydrogen absorption to stimulate solid state disbonding interactions when in the presence of host metal atoms and atomic hydrogen in the solid [50]. The point of the present discussion is to suggest that the accumulated impurities may be responsible for the presence of hydrogen in the grain boundaries, but this does not guarantee embrittlement.

Given all of the above, some of the elements which may be involved in the intergranular embrittlement of nickel are shown in the sequence in Fig. 15. Recent studies (see reference 51 for a review) suggest that yielding begins in the surface grains of polycrystals through the action of dislocation sources near the free surface. The result is that one expects that some hydrogen is dragged into the interior along with mobile dislocations which may then interact with grain boundaries (Fig. 15a,b). Some hydrogen is likely to enter the solid at other than poisoned grain boundaries, evidence for which is the fact that serrated yielding has been observed in large-grained polycrystals and in similar experiments with monocrystals [52] cathodically charged and deformed simultaneously. The latter suggests that dislocations–solute (hydrogen) interactions occur. Likewise, atomic hydrogen which, as described earlier, presumably enters the solid preferentially at grain boundary intersections with the free surface may diffuse via the grain boundaries into the solid. In the later stages of deformation, internal dislocation sources become operational and the incidence of dislocation interactions with the grain boundaries increases. It is conceivable, for example, that dislocations generated by sources located at grain

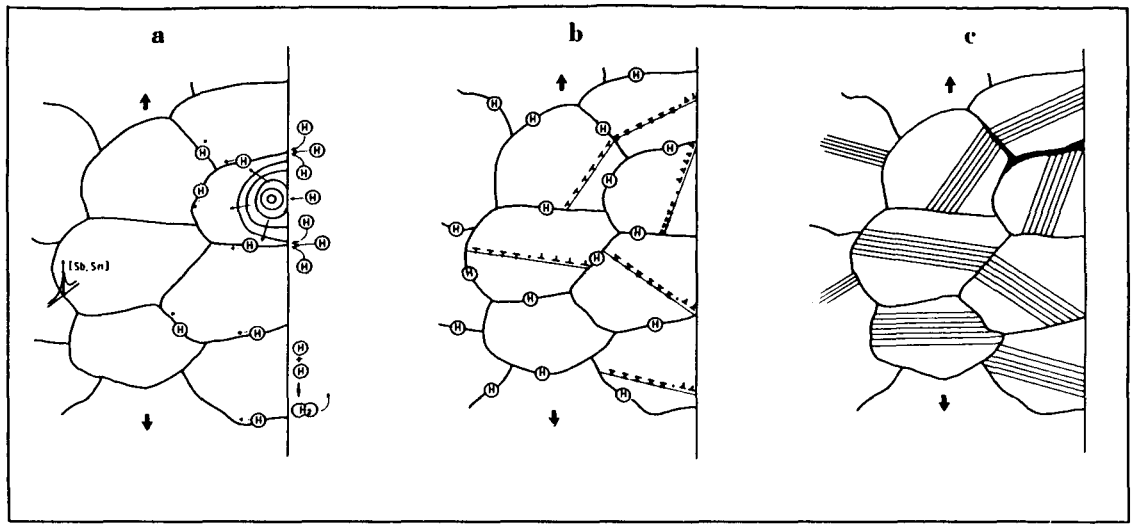

Fig. 15. Schematic showing sequence perhaps involved in intergranular hydrogen embrittlement [4].

boundaries may sweep hydrogen into the bulk. The attendant stress and the presence of hydrogen in the vicinity of the grain boundaries may subsequently lead to embrittlement (Figure 15c) perhaps as a result of the hydrogen–metalloid-induced reduction in the strength of atomic bonds at regions of stress concentration. Though we have studied each aspect of the foregoing, work on dislocation transport has been reported elsewhere [53,54] and will not be described here.

In order to experimentally examine the absorption of hydrogen at metalloid-segregated grain boundaries, one would like to explicitly study the behavior of the grain boundary–electrolyte interface with regard to the hydrogen evolution/absorption processes. Obviously, this is difficult to do *in situ*. On the other hand, we have recently explored the use of metallic glasses as a structural and chemical analog of segregated grain boundaries in electrolytic hydrogen permeation studies [55]. Structurally, Ashby et al. [56] have pointed out that grain boundaries may be described on an atomic scale as a packing of polyhedra, a model which has been used as well to effectively characterize the structure of metallic glasses [57]. In effect, both grain boundaries and metallic glasses may be considered to possess a certain short range order on an atomic scale, but not the long range periodicity typical of perfect crystals. Chemically the transition metal–metalloid type glasses (typically 80 at wt% transition metals, 20 at wt% metalloid compositions) are of compositions that are good approximations of the chemistry of solute segregated grain boundaries in polycrystalline metals and alloys. As mentioned earlier, grain boundary segregation of phosphorus has been observed in thermally treated nickel-base alloys such as Inconel 600 and Hastelloy C-276. Hence, Ni–P binary glasses may be considered to be good structural and chemical analog of grain boundaries in thermally treated nickel-base alloys.

The results of permeation experiments on polycrystalline, high purity nickel, a $Ni_{92.7}Si_{4.5}B_{2.8}$ glass, and $Ni_{81}P_{19}$ glass are given in Fig. 16. The work on $Ni_{81}P_{19}$ was intended to address the case of the metallic glass analog of phorphorus-segregated grain boundaries in nickel-base alloys. In effect, as described earlier with reference to Figure 13, it has been proposed that the segregated grain boundaries might act as preferential paths for the entry of hydrogen into the polycrystalline matrix. Notice that as the charging current increases the steady state permeation current also increases, but far more rapidly for the metalloid-concentrated glass as expected. This suggests, given the grain boundary–metallic glass analog, that the introduction of substantially more hydrogen occurs along

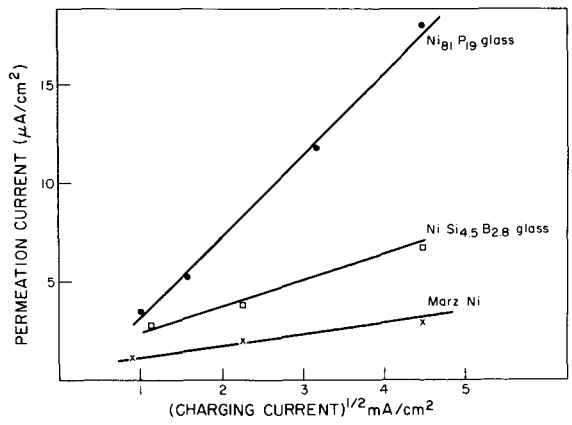

Fig. 16. Steady state permeation flux as a function of changing current for various crystalline and glassy nickel-base materials [55].

metalloid-segregated grain boundaries than via the bulk.

In situ observations which suggest grain boundary transport of hydrogen in nickel have been reported by Tsuru and Latanision [58] using the ion microprobe. In this work, the surface of a polycrystalline specimen of nickel was examined by IMA. The charging time was too short to allow hydrogen to permeate the specimen by lattice diffusion. The result of a step scan analysis of 60_{Ni+} and 1_{H+} (10 μm each step and 13 μm resolution) is shown in Fig. 17 in which three hydrogen peaks can be seen. This suggests that there were spots where the concentration of hydrogen was very large compared with the matrix. Fig. 18 shows the sputtered surface where the IMA measurement was performed and the line of circles which corresponds to the trace of the IMA spot measurements. These peaks correspond to the points of intersection of the IMA scan direction vector with grain boundaries in the specimen as shown in Fig. 18. In essence, the concentration of hydrogen at grain boundaries was found to be very large compared to background hydrogen. Notice as well that the nickel signal is little affected in crossing grain boundaries, that is, the ratio $1_{H+}:60_{Ni+}$ increases significantly. These observations are consistent with the suggestion of grain boundary diffusion that emerged from electrolytic permeation experiments, which suggest that the grain boundary diffusivity of hydrogen is about 60 times faster than that of lattice diffusion [58]. Work supporting these observations has been presented elsewhere [59].

3.3.2. The Effect of Grain Boundary Carbide Morphology on Hydrogen Embrittlement. Lee [60] has studied the case of intergranular embrittlement in

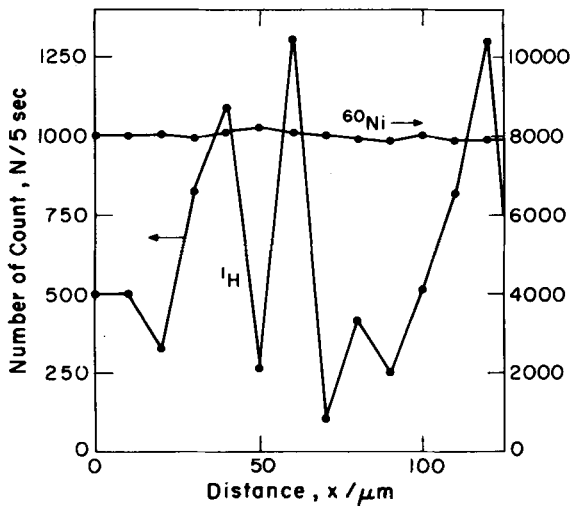

Fig. 17. IMA data showing the increased hydrogen concentration at grain boundaries on the exit surface of a nickel specimen cathodically charged for 2 h at the opposite or entry surface (cathode) [58].

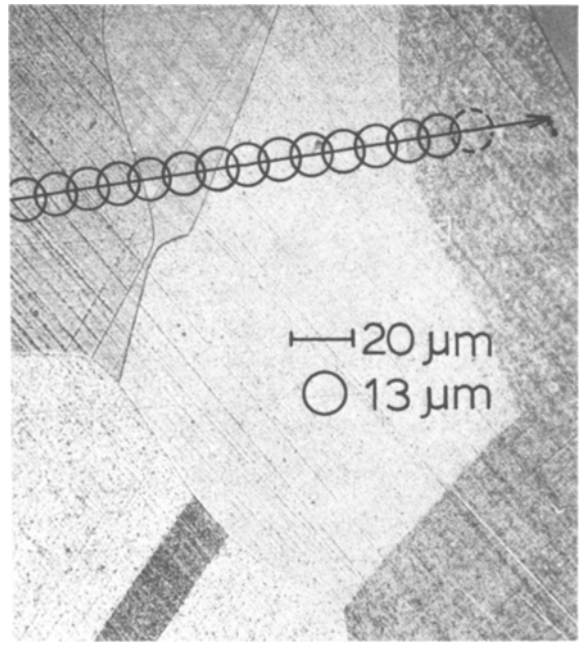

Fig. 18. IMA scanning direction superimposed on the optical micrograph of the surface corresponding to Fig. 16. The hydrogen peaks in the Fig. 16 correspond to grain boundary intersections [58].

which grain boundary carbide morphology plays a more important role than either chromium depletion or solute segregation in the proximity of the grain boundaries. Figure 19 shows the dependence of the ductility (%RA) of Inconel 600 as a function of aging temperature following a solution anneal at 1100° C for 1 h. The separation between the two curves, the lower

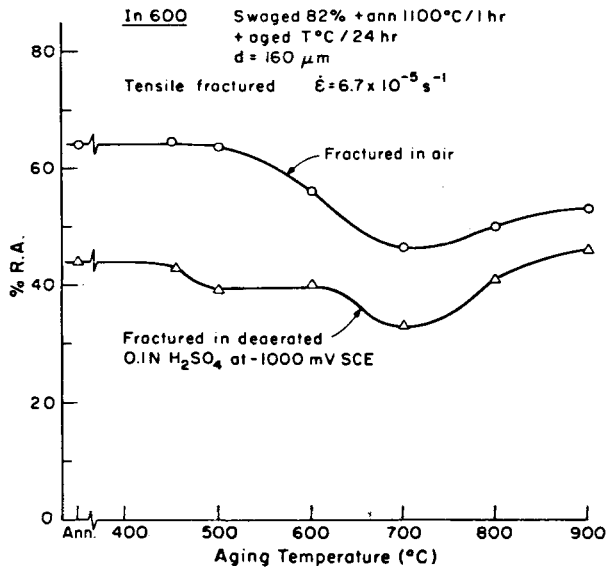

Fig. 19. Ductility as expressed as percent reduction in area (%RA) of Inconel 600 as a function of aging temperature and hydrogen absorption [60].

of which corresponds to specimens that were deformed while being electrolytically charged with hydrogen at −1000 mV(SCE) in 0.1 N H_2SO_4, represents the loss in ductility that is caused by absorbed hydrogen. Notice that an aging ductility loss occurs when specimens are aged at 700° C for 24 h even in the absence of absorbed hydrogen. The effects of hydrogen charging and thermal aging are more clearly shown in Fig. 20 in which reduction-in-area loss is shown as a function of temperature. Note that aging embrittlement, in the absence of absorbed hydrogen, is a maximum following a 700° C anneal for 24 h. Ductility loss due to hydrogen passes through a maximum at an aging temperature of about 500° C. Aging embrittlement due to grain boundary carbide precipitation finds support in the work of Lee and Vermilyea [61]. The variations in the two embrittlement phenomena with aging temperature are best explained by the morphology change in carbide precipitation. A semicontinuous carbide precipitate on grain boundaries such as is produced by 700° C aging causes most severe loss of air ductility and induces intergranular rupture. Carbide precipitates also trap hydrogen and would increase or decrease the effect of hydrogen, depending on the morphology of the precipitation. A thin, continuous grain boundary precipitate traps hydrogen and distributes it uniformly along the grain boundaries, resulting in enhanced intergranular hydrogen embrittlement (500° C aging). Discrete precipitates on grain boundaries and in the matrix trap hydrogen at discontinuous sites, resulting in reduced hydrogen embrittlement (900° C aging). In a microstructure free of precipitates (solution annealed), hydrogen induces intergranular decohesion and some amount of quasi-cleavage in Inconel 600. In the presence of carbide precipitates (solution annealed and aged), hydrogen tends to enhance the existing microvoid coalescence fracture initiated around carbide particles, whether on grain boundaries or in the matrix, causing early failure.

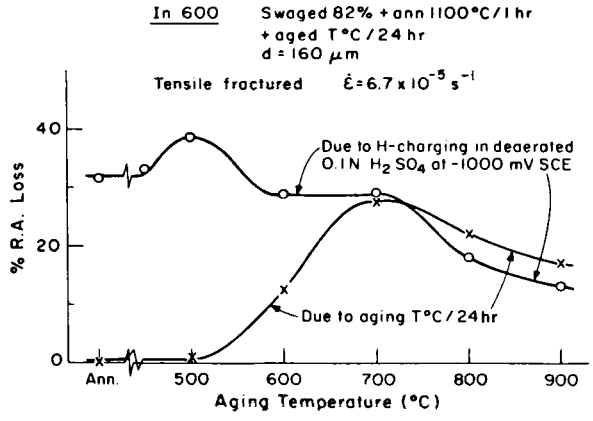

Fig. 20. As in Fig. 18, but showing ductility loss [60].

The aforementioned dependence of fracture characteristics on precipitate morphology is shown in Figs. 21 and 22. Figure 21 shows fractographs of solution-annealed Inconel 600 obtained after testing in the presence of cathodic hydrogen charging. Hydrogen-induced intergranular cracking and quasi-cleavage are shown. The grain face shown in Figure 21(a) is essentially smooth with extensive superimposed slip line traces, an indication that significant plastic flow occurs during grain boundary separation. If Inconel 600 is solution annealed and aged at 700° C for 24 h (Fig. 22) mixed mode intergranular and transgranular fracture occurs when the specimen is deformed to failure in the laboratory atmosphere as well as in the presence of absorbed hydrogen although intergranular failure becomes more dominant in the latter case. It is interesting that the grain faces of the 700° C aged alloy have a rough appearance, unlike the grain faces

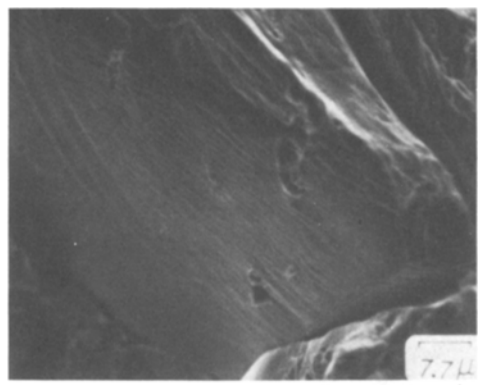

a

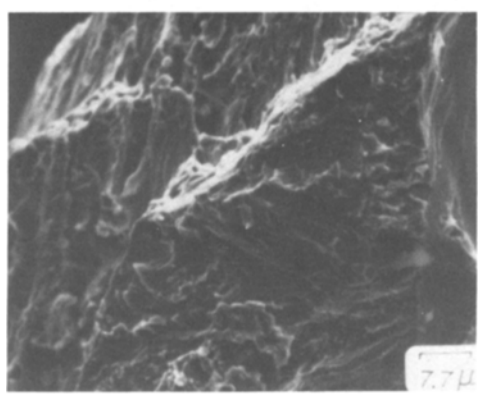

b

Fig. 21. Scanning electron micrographs of solution annealed (1100° C for 1 h) Inconel 600 fractured during hydrogen charging showing (a) smooth intergranular faces and (b) quasi-cleavage [60].

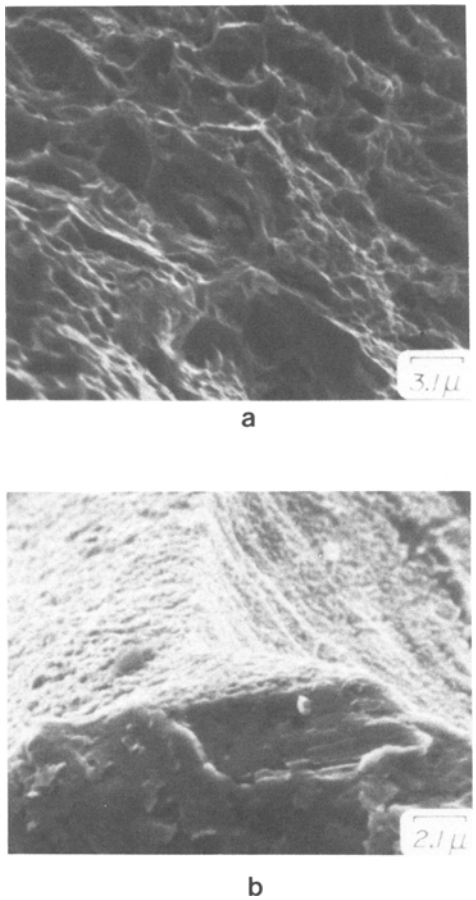

Fig. 22. SEM fractographs of solution annealed and aged (1100° C for 1 h followed by 700° C for 24 h) Inconel 600 fractured during hydrogen charging showing (a) transgranular dimpled area, and (b) grain faces with rough appearance [60].

produced in the solution annealed alloy (Fig. 21). The grain face roughness is likely due to the extensive chromium carbide precipitation that is known to occur when the alloy is aged at 700° C, as described earlier. Figure 23 summarizes in a schematic sense the origin of the fracture morphology observed in this study. It might be mentioned in passing that chromium depletion and P segregation in the vicinity of grain boundaries, both of which may occur during aging, do not seem to affect either this alloy's susceptibility to hydrogen or to aging embrittlement. Lee [60] has also examined Inconel X750 and Incoloy 800 in experiments similar to those described above.

4. ADVANCED PROCESSING

In the preceding discussion emphasis was placed on the recognition that the corrosion resistance of nickel-base alloys is intimately associated with the microstructure of these alloys. Materials processing plays a central role in determining the microstructure of such alloys and, correspondingly, their properties and performance under service conditions. Perhaps the most promising advanced processing technology in this regard is rapid quenching or rapid solidification processing (RSP).

Liquids of virtually any composition may be rapidly quenched to produce metastable solids. Some liquids, with specific composition, however, are glassy in the solid state. In order to achieve a glassy structure, transition metal–metalloid or metal–metal liquid alloys must be quenched at rates greater than 10^6 °C/s. Alloys produced in this way are termed "glassy" alloys as they generally exhibit metallic phases with no long-range structural order, although over a few atomic distances there may be short-range order. For a more detailed description of the properties of metallic glasses, readers are referred to the various books and conference proceedings on this subject [62–64].

Considerable interest has developed in terms of the chemical properties of rapidly quenched glassy alloys, some of which are remarkably inert [65,66]. There is, however, a second family of alloys pro-

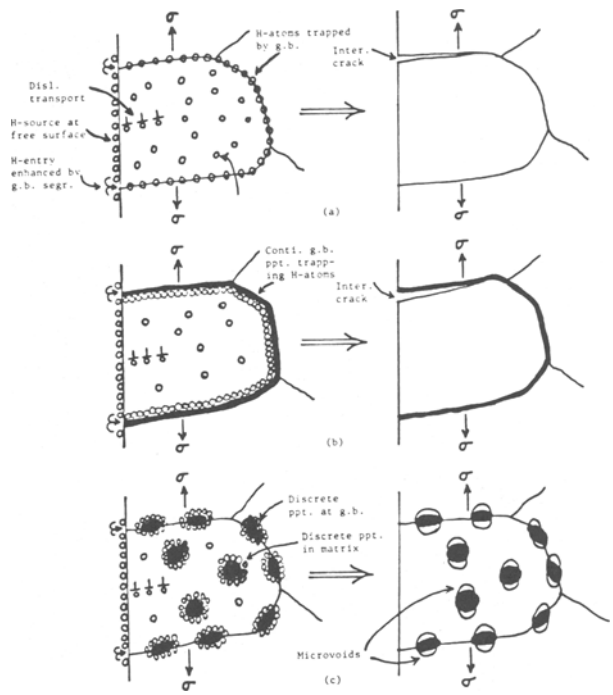

Fig. 23. Schematic illustrating the interaction of transported hydrogen with various traps leading to different hydrogen-induced fracture modes: (a) hydrogen trapped by grain boundaries leading to boundary decohesion; (b) hydrogen trapped by continuous, incoherent precipitates along grain boundaries leading to interface decohesion; and (c) hydrogen trapped by discrete incoherent precipitates at grain boundaries and in the matrix leading to microvoid formation around the precipitate particles [60].

cessed by rapid quenching. In this category are alloys of virtually any composition that are, for example, quenched into the form of thin strips (or atomized to produce powder), subsequently compacted together, and finally hot extruded into the form of sections of rather large sizes. The alloys processed in this way are not amorphous but have grain size of the order of a micron. Likewise, because of rapid solidification, they are chemically more homogeneous than conventionally processed alloys of the same composition. Such materials are often remarkably stable with regard to grain growth at elevated temperatures, a characteristic which Yurek et al. [67] have shown to be critically important in the resistance of RSP type 304 stainless steel in high temperature, oxidizing environments typical of gas turbines.

Although RSP of nickel-base superalloys has received considerable attention [68], little information appears to be available with regard to the aqueous corrosion resistance of such alloys. On the other hand, the chemical properties of RSP crystalline iron- and aluminum-base alloys have been examined at MIT and are summarized in recent publications [69,70]. In general, the findings are very encouraging indeed. Tsuru et al. [70] have investigated the corrosion resistance of compacted and hot extruded austenitic and duplex stainless steel foils produced by rapid solidification of commercial alloys. The extrusion temperature of 1065° C resulted in a microcrystalline structure with a uniform grain size of 2–5 μm. Polarization data in Na_2SO_4–H_2SO_4 solutions revealed little difference in behavior between the wrought and microcrystalline material of the same composition, as shown in Figure 24. However, the microcrystalline alloys were

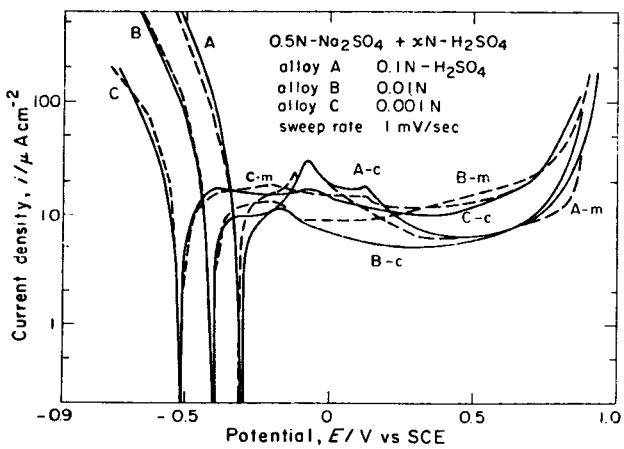

Fig. 24. Polarization curves for microcrystalline alloys (m, dashed) and conventional alloys (c, solid). Alloy A: 20%Cr–18%Ni–6.1%Mo (Avesta 254 SMO); Alloy B: 19%Cr–5%Ni–2.8%Mo (Avesta 3RE60); Alloy C: 23%CR–5%Ni–1.5%Mo (NAS 45M) [70].

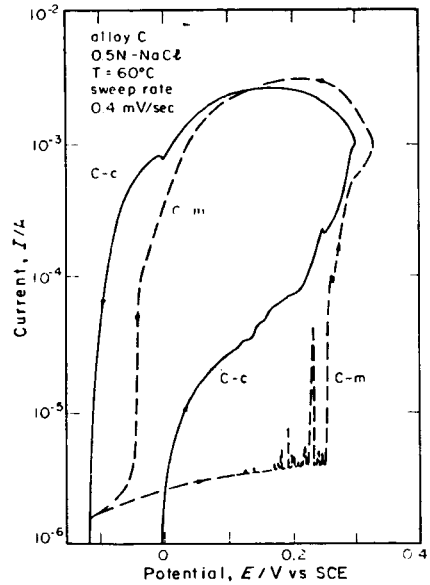

Fig. 25. Anodic polarization curve for alloy C (23%Cr–5%Ni–1.5%Mo; NAS 45M) in 0.5N NaCl at 60° C. Direction of sweep was reversed at 1 mA. Microcrystalline alloy (m, dashed) and conventional alloy (c, solid) [70].

found consistently to be more resistant to pitting than the conventional alloys of the same composition. The improved resistance to pitting of the microcrystalline alloys was thought to be influenced by the more uniform distribution of impurities minimizing segregation or accumulation to form active initiation sites for localized attack. Figure 25 shows polarization diagrams for a wrought and microcrystalline Fe–Cr–Ni–Mo stainless steel in a chloride-containing environment clearly showing the more noble breakdown and protection potentials of the rapidly solidified alloys. Initial stress corrosion tests on the compacted austenitic stainless steel foils are also encouraging, although interference from prior foil boundaries in the crack extension process does compromise properties to a certain extent [71].

In short, while little reported work on the corrosion resistance of RSP nickel-base alloys appears to be available, there is precedent in other alloy systems to suggest that the microstructural control, the extended solubility limits, the homogeneity, and so on, of metastable alloys of nickel would improve the resistance of such alloys to general and localized forms of corrosion. The opportunity presented by RSP for improvement in the performance of nickel-base alloys in service environments of all kinds warrants attention.

5. ACKNOWLEDGMENTS

It is a great pleasure to acknowledge the generous and continuous support for research at MIT provided over

several years by the International Nickel Company through an INCO Fellowship. This Fellowship has provided partial support for doctoral students such as Gary Was, Bill Moshier, and Jerry Frankel during the course of their Sc.D. research in The H.H. Uhlig Corrosion Laboratory at MIT. Likewise, I am happy to acknowledge the Shell Companies Foundation, the Electric Power Research Institute, and the U.S. Office of Naval Research for their support and encouragement of our work on the corrosion of nickel and nickel-base alloys. Finally, grateful thanks are extended to my colleagues Ron Ballinger, Regis Pelloux, Greg Yurek, and Professor H.H. Uhlig for many conversations about various aspects of this work.

5. REFERENCES

1. R.G. Ballinger, ASM Conference: Corrosion of Nickel Base Alloys, Cincinnati, OH, 23–25 October, 1984.
2. G.S. Was, H.H. Tischner, and R.M. Latanision, *Met. Trans, 12A*, p. 1397, 1981.
3. A.W. Thompson, ASM Conference: Corrosion of Nickel Base Alloys, Cincinnati, OH, 23–25 October, 1984.
4. R.M. Latanision and H. Opperhauser, Jr., *Met. Trans., 5*, p. 483, 1974.
5. J.S. Armijo, *Corrosion, 24*, p. 24, 1968.
6. D.A. Vermilyea, C.S. Tedmon, and D.E. Broucher, *Corrosion, 31*, p. 222, 1975.
7. M.H. Brown, *Corrosion, 29*, p. 384, 1973.
8. M. Guttmann, in *Advances in Mechanics and Physics of Surfaces*, vol. 1, p. 1. Harwood Academic Publishers, Chur, Switzerland, 1981.
9. R.H. Jones, M.J. Danielson, and D.R. Baer, ASM Conference: Corrosion of Nickel Base Alloys, Cincinnati, OH, 23–25 October, 1984.
10. Ya.M. Kolotyrkin and O.V. Kasprova, in *Corrosion and Corrosion Protection*, p. 186. Electrochemical Society, Pennington, 1981.
11. C.L. Briant, *Corrosion, 36*, p. 487, 1980.
12. G.P. Airey, "Optimization of Metallurgical Variables to Improve the Stress Corrosion Resistance of Inconel 600," EPRI Eighth Quarterly Report for RP1708-1, 1981.
13. L. Ljungberg, EPRI International Workshop on Low Temperature Sensitization, Paper No. 5, Jan. 21–11, 1982.
14. R.G. Ballinger, R.M. Latanision, W.C. Moshier, and K.N. Siebein, in *Proc. 9th Intl. Cong. on Metallic Corrosion*, vol. 3, p. 265, NRC, Ottawa, 1984.
15. C. Stawstrom and M. Hilbert, *JISI*, p. 77, 1969.
16. E.N. Pugh, ASM Conference: Corrosion of Nickel Base Alloys, Cincinnati, OH, 23–25 October, 1984.
17. R. Bandy and D. Van Rooyen, ASM Conference: Corrosion of Nickel Base Alloys, Cincinnati, OH, 23–25 October, 1984.
18. D.J. Duquette, ASM Conference: Corrosion of Nickel Base Alloys, Cincinnati, OH, 23–25 October, 1984.
19. A.W. Thompson, ASM Conference: Corrosion of Nickel Base Alloys, Cincinnati, OH, 23–25 October, 1984.
20. G.S. Was, H.H. Tischner, R.M. Latanision, and R.M. Pelloux, *Met. Trans., 12A*, p. 1409, 1981.
21. R.G. Ballinger, Sc.D. Thesis, MIT, 1982.
22. W.C.J. Moshier, Sc.D. Thesis, MIT, 1983.
23. D. Van Rooyen, *Corrosion, 31*, p. 327, 1975.
24. W.E. Berry, *Materials Performance, 6*, p. 9, 1984.
25. R. Bandy and D. Van Rooyen, in *Proc. 9th Intl. Cong. on Metallic Corrosion*, vol. 3, p. 202, NRC, Ottawa, 1984.
26. L. Abrego, D.H. Ender, and J.W. Kochera, in *Materials for Energy Systems*, ASM, in press.
27. R. Bandy and D. Van Rooyen, *Corrosion, 40*, p. 281, 1984.
28. J. Blanchet, H. Coriou, L. Grall, C. Mahieu, C. Otter, and G. Turluer, in *Stress Corrosion Cracking and Hydrogen Embrittlement of Iron-Base Alloys*, p. 1149. NACE, Houston, 1977.
29. G.P. Airey, EPRI Report, N.P. 2093, Oct. 1981; N.P.-1354, March 1980.
30. R. Bandy and D. Van Rooyen, *Corrosion, 40*, p. 425, 1984.
31. B.J. Berkowitz and R.D. Kane, *Corrosion, 36*, p. 24, 1980.
32. A.I. Asphahani, *Second Intl. Cong. on Hydrogen in Metals*, paper 3C-2, Paris, 1977.
33. A.I. Asphahani and H.M. Tawancy, in *Corrosion and Corrosion Protection*, p. 154, ECS, Pennington, 1981.
34. A.I. Asphahani, Paper No. 42, Corrosion '78 Conference, NACE, 1978.
35. R.J. Coyle, Jr., J.A. Kargol, and N.F. Fiore, *Met. Trans., 12A*, p. 653, 1981.
36. J.W. Kochera, A.K. Dunlop, and J.P. Tralmer, Paper No. 50, Corrosion '76 Conference, NACE 1976.
37. K. Balajiva, R.N. Cook, and D.K. Worn, *Nature, 178*, p. 433, 1956.
38. R. Speiser and J.W. Spretnak, *Stress Corrosion Cracking and Embrittlement*, Wiley, New York, 1956, p. 92.
39. H.L. Marcus and P.W. Palmberg, *Trans. AIME, 245*, p. 1664, 1969.
40. D.F. Stein, A. Joshi, and R.P. Laforce, *Trans. ASM, 62*, p. 776, 1969.
41. K. Yoshino and C.J. McMahon, Jr., *Met. Trans., 5*, p. 363, 1974.
42. R.O. Ritchie, *Met. Trans., 8A*, p. 1131, 1977.
43. A. Joshi and D.F. Stein, *Met. Trans., 1*, p. 2543, 1970.
44. A. Joshi and D.F. Stein, *J. Inst. Metal, 99*, p. 178, 1971.
45. J.M. Popplewell and J.A. Ford, *Met. Trans., 5*, p. 2600, 1974.
46. C.L. White, L. Heatherly, and R.A. Padgett, *Acta Met., 31*, p. 111, 1983.
47. R.O. McCright and R.W. Staehle, *J. Electrochem. Soc., 121*, p. 605, 1974.
48. F. Zakroczymski, Z. Szlarska-Smialowska, and M. Smialowski: *Werkstoffe und Korrosion, 27*, p. 625, 1976.
49. J.M. Bruemmer, R.H. Jones, M.T. Thomas, and D.R.

Baer, *Scripta Met, 14*, p. 1233, 1980.
50. M.E. Eberhart, K.H. Johnson, and R.M. Latanision, *Acta Met., 32*, p. 955, 1984.
51. R.M. Latanision in *Surface Effects in Crystal Plasticity*, Noordhoff International Publishing Co., Leyden, 1977, p. 3.
52. R.M. Latanision and R.W. Staehle, *Scripta Met., 2*, p. 667, 1968.
53. M. Hashimoto and R.M. Latanision, in *Proc. 9th Intl. Cong. on Metallic Corrosion*, vol. 4, p. 427. NRC, Ottawa, 1984.
54. G.S. Frankel and R.M. Latanision, in *Proc. 9th Intl. Cong. on Metallic Corrosion*, vol. 4, p. 466. NRC, Ottawa, 1984.
55. R.M. Latanision, C.R. Compeau, and M. Kurkela, in *Proc. Alexander R. Troiano Symposium on Hydrogen Embrittlement and Stress Corrosion Cracking*, p. 297. ASM, Metals Park, OH, 1984.
56. M.F. Ashby, F. Spaepen, and S. Williams, *Acta Met., 26*, p. 1647, 1978.
57. D.E. Polk, *Scripta Met., 4*, p. 117, 1970.
58. T. Tsuru and R.M. Latanision, *Scripta Met., 16*, p. 575, 1982.
59. T. Schober and C. Dieker, *Met. Trans., 14A*, p. 2440, 1983.
60. T.S.F. Lee, Sc.D. Thesis, MIT, 1982.
61. D. Lee and D.A. Vermilyea, *Met. Trans., 2*, p. 2565, 1971.
62. N.J. Grant and B.C. Geissen, editors, *Rapidly Quenched Metals*, MIT Press, Cambridge, MA, 1976.
63. J.J. Gilman and H.J. Leamy, editors, *Metallic Glasses*, ASM, Metals Park, OH, 1978.
64. B.J. Berkowitz and R.O. Scattergood, editors, *Chemistry and Physics of Rapidly Solidified Materials*, Metallurgical Society of AIME, Warrendale, PA, 1983.
65. E. McCafferty, C.R. Clayton, and J. Oudar, editors, *Fundamental Aspects of Corrosion Protection and Surface Modification*, Electrochemical Society, Pennington, NJ, 1984.
66. K. Hashimoto and T. Masumoto, in *Amorphorus Material—Physics and Technology*, Bando Printing, Osaka, Japan, 1983, p. 235.
67. G.J. Yurek, D. Eisen, and A. Garratt-Reed, *Met. Trans., 13A*, p. 473, 1982.
68. R.J. Patterson II, A.R. Cox, and E.C. Van Reuth, *J. Metals*, p. 34 Sept. 1980.
69. P.C. Searson and R.M. Latanision, in *Proc. Intl. Conf. on New Developments in Stainless Steel Technology*, p. 7. *ASM*, Metals Park, OH, 1985.
70. T. Tsuru and R.M. Latanision, *J. Electrochem. Soc., 129*, p. 1402, 1982.
71. T. Tsuru, S. Zhang and R.M. Latanision, *Proc. 4th Intl. Conf. on Rapidly Quenched Metals*, p. 1437, Sendai, Japan, 1981.